

**Shining Light on Dark Matter,  
One Photon at a Time**

by

Brandon Leigh Allen

Submitted to the Department of Physics  
in partial fulfillment of the requirements for the degree of

Doctorate of Science in Physics

at the

MASSACHUSETTS INSTITUTE OF TECHNOLOGY

June 2019

© Massachusetts Institute of Technology 2019. All rights reserved.

Author .....  
Department of Physics  
May 18, 2019

Certified by .....  
Christoph E.M. Paus  
Professor  
Thesis Supervisor

Accepted by .....  
Nergis Mavalvala  
Associate Department Head for Education



# Shining Light on Dark Matter, One Photon at a Time

by

Brandon Leigh Allen

Submitted to the Department of Physics  
on May 18, 2019, in partial fulfillment of the  
requirements for the degree of  
Doctorate of Science in Physics

## Abstract

A search is conducted for new physics in final states containing a photon and missing transverse momentum in proton-proton collisions at  $\sqrt{s} = 13$  TeV. The data collected by the CMS experiment at the CERN LHC correspond to an integrated luminosity of 35.9 inverse femtobarns. No deviations from the predictions of the standard model are observed. The results are interpreted in the context of dark matter production and limits on new physics parameters are calculated at 95% confidence level. For the two simplified dark matter production models considered, the observed (expected) lower limits on the mediator masses are both 950 (1150) GeV for 1 GeV dark matter mass.

Thesis Supervisor: Christoph E.M. Paus  
Title: Professor



## Acknowledgments

This is the acknowledgements section. You should replace this with your own acknowledgements.



# Contents

<b>1</b>	<b>Global Event Reconstruction</b>	<b>9</b>
1.1	Particle Flow Elements . . . . .	11
1.1.1	Tracks . . . . .	11
1.1.2	Primary Vertexing . . . . .	12
1.1.3	Secondary Vertexing . . . . .	13
1.1.4	ECAL Superclusters . . . . .	13
1.1.5	HCAL Clusters . . . . .	14
1.1.6	Muon Segments . . . . .	15
1.1.7	Isolation . . . . .	15
1.2	Particle Identification . . . . .	16
1.2.1	Muons . . . . .	16
1.2.2	Electrons . . . . .	17
1.2.3	Isolated Photons . . . . .	18
1.2.4	Hadrons and Nonisolated Photons . . . . .	18
1.3	Event Variables . . . . .	18
1.3.1	Jets . . . . .	18
1.3.2	Missing Tranverse Energy . . . . .	18





# Chapter 1

## Global Event Reconstruction

In the previous chapter, we discussed the interactions of particles with the individual subdetectors and how these generate electrical signals. Now, we shall discuss the reverse process, namely reconstructing the individual particles or physics objects from the electrical signals recorded by the subdetectors.

Traditionally, each class of physics object is reconstructed using information from a single subdetector: muons from the muon chambers, isolated photons and electrons from the ECAL, jets and missing transverse energy from the HCAL, and secondary vertices from  $\tau$  lepton and  $b$  hadron decays from the tracker. However, as depicted in Figure 1-1, each type of particle interacts with multiple different subdetectors and this information is lost unless the information from all the subdetectors is combined into a single global event description.

The particle flow (PF) algorithm leverages the fine angular granularity of the calorimeters and the excellent momentum resolution of the inner tracker and muon chambers to greatly improve the reconstruction of physics objects and include soft particles that would otherwise be ignored. This is especially advantageous for jet energy measurements as roughly 62% of the jet energy is carried by charged hadrons, approximately 27% by photons, around 10% by neutral hadrons, and about 1.5% by neutrinos.

The distinguishing feature of the PF algorithm is to combine multiple detector signals together into a single PF candidate. The input detector signals are the tracks,

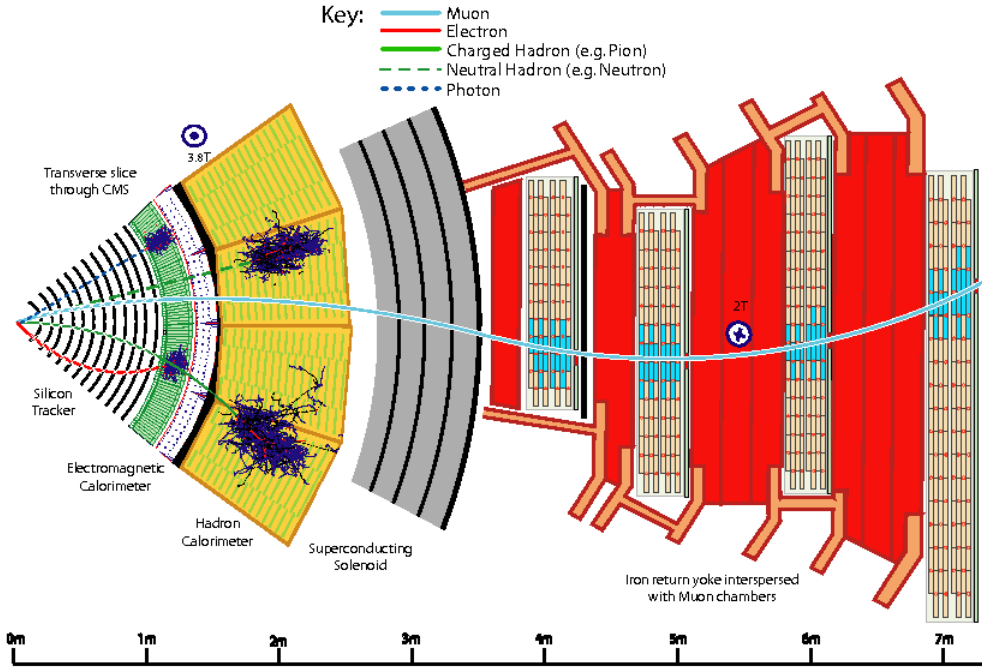


Figure 1-1: A sketch of a transverse slice of the CMS detector showing particle interactions from the interaction point to the muon detector. Reprinted from Reference [1].

vertices, calorimeter clusters, and muon segments described in Section 1.1. Based on their proximity in the  $\eta$ - $\phi$ , these PF elements are combined into muons, electrons, photons, and hadrons. Muon segments are combined with inner tracks to produce muons, inner tracks are combined with calorimeter clusters to produce electrons and charged hadrons, and calorimeter clusters are correlated to produce photons and neutral hadrons.

The PF algorithm reconstructs particles in the blocks described in Section 1.2 and after each block any PF elements associated to a PF candidate are not considered by the following blocks. For example, clusters associated with photons will not be used when reconstructing neutral hadrons. After all PF candidates are identified, they can be combined into event-wide variables such as jets and the missing transverse energy as described in Section 1.3.

## 1.1 Particle Flow Elements

### 1.1.1 Tracks

The Combinatorial Track Finder software is used to reconstruct tracks in an iterative inside-out process. Initial iterations search for tracks that are easy to find, e.g. those with high  $p_T$ , and hits associated with these tracks are removed for later iterations, reducing the combinatorial complexity and simplifying the search for more difficult tracks, e.g. greatly displaced ones.

The first step is to form seeds based on pixel hits, double strip hits containing 3D information, and an estimate of the beam spot. Earlier iterations require three pixel hits while later iterations gradually loosen the requirements. The final iterations specifically target increased muon tracking efficiency by including information from the muon chambers.

Next, a Kalman filter is used to find additional hits consistent with the evolution of the track seeds through the rest of the tracker, accounting for the magnetic field, energy loss due to ionization, and multiple scattering. The five parameters used for the helical trajectory evolution are the curvature  $\rho$ , the azimuthal angle  $\phi_0$ , the transverse impact parameter  $d_0$ , the longitudinal impact parameter  $z_0$ , and  $\lambda = \cot \theta$ , where  $\theta$  is the polar angle.

After propagating the track through all layers of the detector and finding all associated hits, a Kalman fitter and smoother is used to refit the overall trajectory while a fourth-order Runge-Kutta method is used to extrapolate the trajectory between successive hits. To reduce the fraction of fake tracks, various quality requirements concerning the number of missing hits, the reduced  $\chi^2$  of the fit, and compatibility with a primary vertex are applied before proceeding to the next iteration.

Track reconstruction for electrons is more complicated as the Kalman filter is not a good description because of the high rate of non-Gaussian energy loss due to brehmsstrahlung these tracks experience within the tracker. To improve the electron reconstruction efficiency, the electron seed collection is filled both by looking outside-in for ECAL superclusters (see Section 1.1.4) consistent with track seeds and inside-

out track seeds consistent with superclusters. A Gaussian Sum Filter (GSF) defined to approximate the Bethe-Heitler energy-loss distribution is used to fit the trajectory of electron tracks.

### 1.1.2 Primary Vertexing

A deterministic annealing (DA) algorithm is used to associate tracks to primary vertices. Tracks must pass additional requirements on the transverse impact parameter  $d_0$ , the number of strip and pixel hits, and the reduced  $\chi$  of the trajectory fit to be considered when finding primary vertices. The most probable vertex positions at an artificial temperature  $T$  are determined by the minimization of the “free energy”

$$F = -T \sum_i^{N_T} \ln \sum_j^{N_V} p_{ij} \rho_j \exp \left[ -\frac{1}{T} \left( \frac{z_i^T - z_j^V}{\sigma_i^z} \right)^2 \right] \quad (1.1)$$

where the  $z_j^V$  are the vertex positions with weights  $\rho_j$ , the  $z_i^T$  and  $\sigma_i^z$  are the longitudinal impact parameters and the corresponding uncertainties of the tracks, and the  $p_{ij}$  are the probabilities of assigning the track  $i$  of  $N_T$  to the vertex  $j$  of  $N_V$ .

The DA algorithm starts with a single vertex at a very high temperature that is gradually decreased. The free energy  $F$  is minimized with respects to  $z_j^K$  at each new temperature and a vertex is split in two whenever  $T$  falls below its critical temperature

$$T_C^j = 2 \sum_i \frac{p_i p_{ij}}{(\sigma_i^z)^2} \left( \frac{z_i^T - z_j^V}{\sigma_i^z} \right)^2 \bigg/ \sum_i \frac{p_i p_{ij}}{(\sigma_i^z)^2}. \quad (1.2)$$

The annealing procedure with vertex splitting continues down to  $T = 4$  and the final assignment of tracks to vertices is performed at  $T = 1$  without any further splitting. The vertex designated as *the* primary vertex of the hard scattering is the one which maximizes

$$\sum_i (p_T^i)^2 + (p_T^{\text{miss}})^2, \quad (1.3)$$

where  $p_T^i$  is the transverse momentum of a track assigned to the vertex and  $p_T^{\text{miss}}$  is the magnitude of the momentum imbalance in the transverse plane for the vertex.

### 1.1.3 Secondary Vertexing

Long-lived particles such as  $b$  hadrons and  $\tau$  leptons often produce charged particles in their decays. These charged particles are traced to a secondary vertex at the location of the decay, which is identified by the inclusive vertex fitter (IVF) algorithm.

The IVF procedure begins by selecting seed tracks with a 2D impact parameter significance  $\sigma_{d_0} \geq 1.2$  and a 3D impact parameter  $\sqrt{d_0^2 + z_0^2} \geq 50 \mu\text{m}$ . Tracks are assigned to a secondary vertex based on their opening angle with the seed track and distance at closest approach, with the additional stipulation that this distance be smaller for the secondary vertex than for the primary vertex.

To determine the precise position of the secondary vertices, the associated tracks are fitted with the adaptive vertex fitter and any vertices with a flight distance significance less than a certain threshold are discarded. At this point, a track is unassociated from a secondary vertex if the angular distance between the track and the secondary vertex flight direction is greater than 0.4 and if the track's distance at closest approach is larger than the magnitude of its impact parameter.

The secondary vertex position is refitted after track cleaning if there are still at least two tracks associated with the vertex. The last stage of cleaning removes a secondary vertex if it shares at least 20% of its tracks with another and the flight distance significance between the two is less than ten.

### 1.1.4 ECAL Superclusters

Due to the large amount of material in the tracker, electrons often emit bremsstrahlung photons, photons often convert to electron-positron pairs, and the bremsstrahlung photons and converted electrons often undergo further conversion and bremsstrahlung before reaching the ECAL. Because of the bending of electron trajectories in the magnetic field, the resulting electromagnetic (EM) shower is significantly spread in the  $\phi$ -direction and collimated in the  $\eta$ -direction. The ECAL reconstruction algorithm combines the basic cluster from each showered particle into a supercluster representing the initial electron or photon from the hard scattering.

The first step is the identification of a seed crystal with greater transverse energy than its immediate neighbors and above a predefined minimum threshold. The energy of each crystal is determined from calibration constants combined with the amplitude and peak time obtained by fitting the pulse shape of the ten time samples surrounding the triggering bunch crossing.

In the barrel, a supercluster starts with a  $5 \times 1$  array of crystals in the  $\eta$ - $\phi$  plane centred on the seed crystal. The array is extended around the seed crystal in the  $\phi$ -direction up to  $|\Delta\phi| \leq 0.3$  if the energy of the additional crystals exceeds a certain threshold. The contiguous array is grouped into distinct basic clusters each containing a seed array with energy greater than another threshold. The supercluster is the collection of basic threshold found in the  $\eta$ - $\phi$  region centered on the initial seed crystal. Since the crystals in the endcaps are arranged in an  $x$ - $y$  grid, clustering here uses fixed  $5 \times 5$  matrices of crystals. After a seed cluster is identified, additional, partially overlapping  $5 \times 5$  matrices are added if their centroid lies within  $|\Delta\eta| \leq 0.07$  and  $|\Delta\phi| \leq 0.3$ . For uncovered photons, both methods produce superclusters that are simple  $5 \times 5$  matrices.

### 1.1.5 HCAL Clusters

The purpose of clustering in the HCAL is to measure the energy and direction of neutral hadrons, disentangle neutral hadrons from charged hadron energy deposits, and improve the energy measurement for charged hadrons with poorly reconstructed tracks. Similar to the supercluster algorithm, a cluster in the HCAL is first identified by a seed cell with greater transverse energy than its immediate neighbors and above a predefined minimum threshold. This seed is then grown into a topological cluster by adding cells with at least a corner in common with a cell already in the cluster and energy above twice the noise threshold.

An iterative Gaussian mixture model is used to break each topological cluster of  $M$  individual cells is broken into  $N$  energy deposits corresponding to individual particles, where  $N$  is the number of seeds. Each energy deposit is modeled as a Gaussian distribution  $\mathcal{N}$  with amplitude  $A_i$ , mean  $\vec{\mu}_i$  in the  $\eta$ - $\phi$  plane, and width

$\sigma$  fixed by the calorimeter resolution. The expected fraction  $f_{ji}$  of the energy  $E_j$  measured in the cell at position  $\vec{c}_j$  from the  $i$ th energy deposit is

$$f_{ji} = \frac{\mathcal{N}(\vec{c}_j|A_i, \vec{\mu}_i, \sigma)}{\sum_k^N \mathcal{N}(\vec{c}_j|A_k, \vec{\mu}_k, \sigma)}. \quad (1.4)$$

The amplitude and position of each energy deposit are determined by an analytical maximum-likelihood fit to be

$$A_i = \sum_j^M f_{ji} E_j \quad \left| \quad \vec{\mu}_i = \sum_j^M f_{ji} E_j \vec{c}_j \quad (1.5)$$

where the initial values are the energy and position of the seeds. The process of calculating energy fractions  $f_{ji}$  and fitting for the amplitudes  $A_i$  and positions  $\vec{\mu}_i$  is repeated until convergence, at which point they are taken as the cluster parameters.

### 1.1.6 Muon Segments

Muon segments are reconstructed from the hits in the muon chambers using a Kalman filter in a similar manner to that described for the inner tracker in Section 1.1.1. A full track constructed in this way is referred to as a standalone muon.

### 1.1.7 Isolation

While not a physics object persay, isolation is a key concept of the PF algorithm used to distinguish prompt leptons and photons originating in the hard scattering from those originating in the decays of hadrons during the parton shower.

$$(I_{\text{CH}} + I_{\text{NH}} + I_\gamma)/p_{\text{T}}^e$$

In the identification criteria, the maximum PF charged hadron isolation  $I_{\text{CH}}^{\text{max}}$  is the maximum of the standard PF charged hadron isolation computed for all reconstructed vertices. Standard PF charged hadron isolation is computed with respect to the primary vertex. Since the object with the highest  $p_{\text{T}}$  in the selected events is typically a photon, which has no intrinsic association to a vertex, it is possible that the identified primary vertex does not correspond to the  $pp$  interaction from which

the photon object originate. In such cases, the photon object can be surrounded by charged hadrons, i.e., a part of a jet, and still appear isolated under the standard charged hadron isolation. The use of maximum isolation is a conservative measure to address such misidentification.

Effective areas for isolations are also recomputed to maintain flat pileup dependence as given in Table 1.1

Table 1.1: Effective areas for isolations.

Isolation	$ \eta  < 1.0$	$1.0 <  \eta  < 1.479$
maximum PF charged hadron isolation	0.01064	0.1026
PF neutral hadron isolation	0.0597	0.0807
PF photon isolation	0.1210	0.1107

## 1.2 Particle Identification

### 1.2.1 Muons

The first block of the PF algorithm reconstructs three types of muon candidates: the standalone muons described in Section 1.1.6, outside-in global muons, and inside-out tracker muons. To construct a global muon, the algorithm identifies an inner track consistent with the trajectory of a standalone muon evolved inwards using a Kalman filter similar to those discussed in Section 1.1.1. After finding a match, a global muon candidate is created by combining the inner track with the standalone track with a second Kalman filter. Conversely, to construct a tracker muon, the algorithm identifies a muon segment consistent with the trajectory of a inner track with  $p_T > 0.5 \text{ GeV}$ . Global and tracker muons sharing the same inner track are merged into a single candidate. For muons with  $p_T < 200 \text{ GeV}$ , the muon momentum is that of the inner track, while the momentum is determined from a global fit of the muon chambers and inner tracker for muons with momentum above this threshold.

Hadrons misidentified muons are rejected through two separate mechanisms. First, the isolation with respects to inner tracks and calorimeter deposits within  $\Delta R < 0.3$



is required to be less than 10% of the muon  $p_T$ . Non-isolated muons are kept only if certain selections on the reduced  $\chi^2$  of the track fit and the two impact parameters  $d_0$  and  $d_z$  are satisfied. Finally, misidentified or misreconstructed muons can lead to a spurious imbalance in the transverse momentum. The procedure used to identify and remove these muon candidates is described in Section 1.3.2. The total efficiency of muon reconstruction is 99%.

The work described in this thesis only considers global muons with  $p_T^\mu > 10 \text{ GeV}$  and  $|\eta^\mu| < 2.5$ . This minimum requirement is only used to reject events containing a muon and is referred to as the veto muon ID. The loose muon ID adds the requirement that the relative combined PF Isolation  $I_{\text{PF}}^{\text{rel.}}$  must be less than 0.25. In order for a muon to pass the tight ID, it must satisfy the following additional requirements:  $p_T^\mu > 30 \text{ GeV}$ , relative combined PF Isolation  $I_{\text{PF}}^{\text{rel.}} < 0.15$ , global-muon track fit reduced  $\chi^2 < 10$ , at least one muon-chamber hit included in the global-muon track fit, muon segments in at least two muon stations, inner track has transverse (longitudinal) impact parameter  $d_0 < 2 \text{ mm}$  ( $d_z < 5 \text{ mm}$ ) with respects to the primary vertex, at least one pixel hit, and more than five tracker layers with hits.

### 1.2.2 Electrons

The work described in this thesis only considers electrons with  $p_T^e > 10 \text{ GeV}$  and  $|\eta^e| < 2.5$ . Additionally, electrons must pass further cuts on the following observables: the  $\sigma_{\text{ini}\eta}$  of the corresponding SC, the  $\Delta\eta$  and  $\Delta\phi$  between the SC seed crystal and the GSF track at the PV, the energy ratio of  $H/E$  of the corresponding ECAL and HCAL towers, the relative combined PF Isolation  $I_{\text{PF}}^{\text{rel.}}$ , the difference in energy measured in the tracker and the calorimeter  $|1/E - 1/p|$ , the number of missing hits in the inner tracker, and the existence of a pair of tracks originating at a displaced vertex, indicting photon conversion. The exact values of the cuts are tuned based on whether the electron is in the barrel or the endcap and to give desired signal efficiencies and background acceptance. The loose ID is tuned to 90% signal efficiency and 0.5% background acceptance, while the tight ID is tuned to 70% signal efficiency and 0.1% background acceptance.

### **1.2.3 Isolated Photons**

text.

### **1.2.4 Hadrons and Nonisolated Photons**

text.

## **1.3 Event Variables**

### **1.3.1 Jets**

### **1.3.2 Missing Tranverse Energy**